Ecotoxicology and Environmental Safety 191 (2020) 110229

Contents lists available at ScienceDirect

Ecotoxicology and Environmental Safety

journal homepage: www.elsevier.com/locate/ecoenv

Mercury isotope compositions in large anthropogenically impacted Pearl River, South China

Yuanyuan Zhang[a,b], Jiubin Chen[a,c,*], Wang Zheng[c], Ruoyu Sun[c], Shengliu Yuan[d], Hongming Cai[c], David Au Yang[a,b], Wei Yuan[c], Mei Meng[c], Zhongwei Wang[a,b], Yulong Liu[a,b], Jianfeng Liu[a,b]

[a] State Key Laboratory of Environmental Geochemistry, Institute of Geochemistry, Chinese Academy of Sciences, Guiyang, Guizhou, 550081, China
[b] University of Chinese Academy of Sciences, Beijing, 100049, China
[c] Institute of Surface-Earth System Science, Tianjin University, Tianjin, 300072, China
[d] Chemistry Department, Trent University, Peterborough, Ontario, K9J7B8, Canada

ARTICLE INFO

Keywords:
Mercury isotope compositions
Isotope tracing
Dissolved load
Pearl river

ABSTRACT

Rivers integrate natural and anthropogenic mercury (Hg), and are important vectors of terrestrial Hg to the oceans. Here, we report the total Hg concentration and Hg isotope compositions of dissolved load in the Pearl River, the second largest river in China, in order to understand the processes and sources affecting Hg systematics in large anthropogenically-impacted river water. The dissolved Hg showed a concentration varying from 0.45 to 2.44 ng/L, within the range reported for natural background lake and river waters. All river water samples showed significantly negative δ^{202}Hg (−2.89‰ to −0.57‰), slightly positive Δ^{200}Hg (−0.05‰ to 0.52‰), and mostly positive Δ^{199}Hg (0.10‰ to 0.57‰), except for three extremely negative values (−2.25‰ to −0.76‰). Combined with other geochemical parameters, we suggest that the influence of in-river processes, such as sorption and reduction, on the Hg isotope compositions is very limited, and the dissolved Hg in the Pearl River mainly comes from atmospheric precipitation and surface soil weathering. Although the whole river basin is largely affected by urban, industrial and mining activities, unlike other heavy metals, their direct contributions to dissolved Hg seem limited. It is worth noting that the three samples with very negative Δ^{199}Hg values (down to −2.25‰) are derived from special source which attribute to the input of Hg released from the local incineration of electronic wastes. This study demonstrates that isotope approach is a powerful tool for tracing sources and pathways of Hg in large complex river systems.

1. Introduction

Mercury (Hg) is a globally distributed toxic heavy metal. It can be transported globally in the atmosphere and deposited via dry or wet deposition (Driscoll et al., 2013; Selin, 2009). The Hg deposited in the aquatic ecosystem can be converted into neurotoxic methylmercury (MeHg), a more toxic Hg form than inorganic Hg, by microbial processes. The MeHg is readily bio-accumulated by low trophic level organisms and further bio-magnified during trophic transfer in aquatic food webs, posing potential threats to the aquatic biota and human health (Beckers and Rinklebe, 2017; Driscoll et al., 2013; Leopold et al., 2010). Therefore, understanding the Hg cycle in aquatic system become necessary to further constrain their impact on the MeHg formation. Rivers are important freshwater systems as they enable the transport of large amount of materials derived from both natural and anthropogenic sources to the ocean (Amos et al., 2014; Emmerton et al., 2013; Zhen et al., 2016). There is an increasing number of studies on Hg concentration and speciation in rivers (Baptista-Salazar et al., 2017; Carroll et al., 2000; Guo et al., 2008; Hissler and Probst, 2006; Wang et al., 2004), but the sources and processes affecting Hg in the river especially large rivers remain poorly unraveled emphasizing the need to constrain them to better understand the Hg global cycle.

Mercury isotope compositions play a critical role in tracing the sources and processes of Hg in the environment. Previous studies have reported mass-dependent fractionation (MDF) and mass-independent fractionation (MIF) of Hg isotopes in atmospheric precipitation (Chen et al., 2012; Foucher et al., 2013; Sherman et al., 2010; Wang et al., 2015; Yuan et al., 2015, 2018), lake water (Chen et al., 2016), aquatic organisms (Blum et al., 2014; Donovan et al., 2016), glacier (Zdanowicz et al., 2016), seawater (Štrok et al., 2015), dissolved and suspended loads and sediments of contaminated rivers (Baptista-Salazar et al., 2018; Blum et al., 2014; Demers et al., 2018; Donovan et al., 2016;

* Corresponding author. Institute of Surface-Earth System Science, Tianjin University, Tianjin, 300072, China.
E-mail address: jbchen@tju.edu.cn (J. Chen).

https://doi.org/10.1016/j.ecoenv.2020.110229
Received 26 November 2019; Received in revised form 14 January 2020; Accepted 16 January 2020

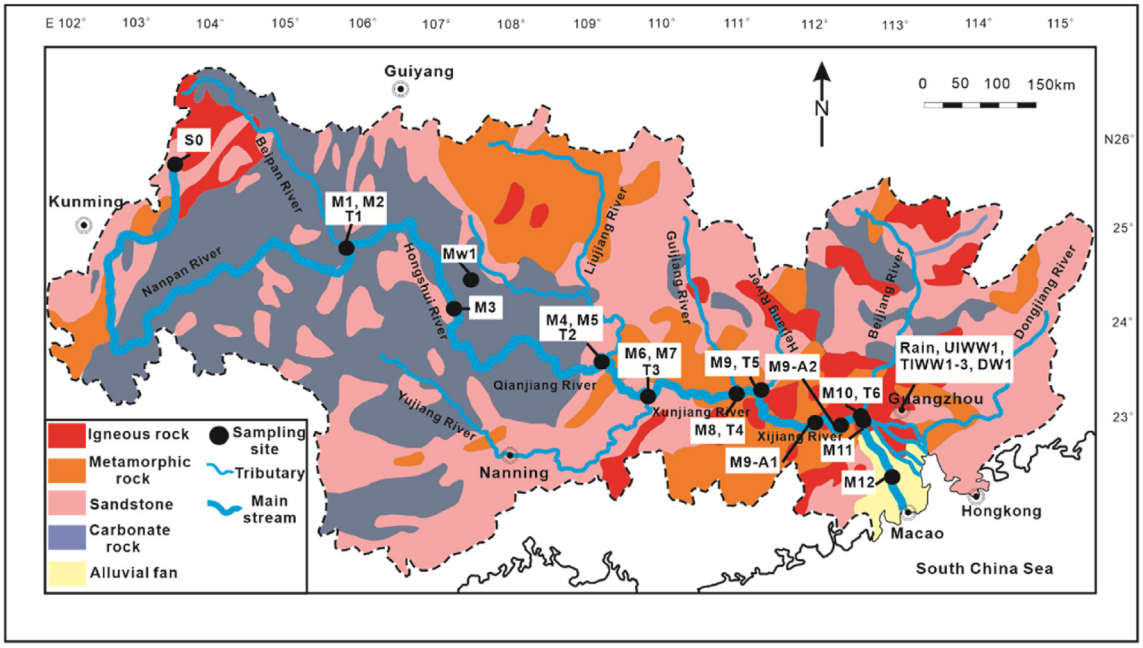

Fig. 1. Study area and location of the sampling sites. Surface water was collected at mainstream (M1 to M12) and tributaries (T1 to T6), spring water (S0) was collected at headwater, rainwater was collected at Guangzhou, mine wastewater Mw1 was collected at Pb and Zn mining industry in Guangxi, untreated industrial wastewater UIWW1 and treated industrial wastewater TIWW1-3 and domestic wastewater DW1 were collected at Guangzhou.

Foucher et al., 2013; Washburn et al., 2017, 2018). Nearly all physical, chemical and biological processes cause MDF (represented by δ^{202}Hg, see details in method) (Blum et al., 2014), but MIF is only caused by a small number of processes. MIF of odd-mass isotopes (odd-MIF) can be caused by magnetic isotope effect (MIE) and nuclear volume effect (NVE) (Bergquist and Blum, 2007; Cai and Chen, 2016), MIE is mainly observed in photochemical reduction of Hg(II) and photo-demethylation of MeHg, whereas NVE is found in some non-photochemical processes such as abiotic dark reduction and liquid-vapor evaporation (Bergquist and Blum, 2007; Estrade et al., 2009; Zheng and Hintelmann, 2009, 2010a, 2010b). Interestingly, the mechanisms responsible for MIF of even-mass isotope (even-MIF) reported in many atmosphere-derived samples remain unknown (Chen et al., 2012a; Sherman et al., 2010; Wang et al., 2015; Yuan et al., 2015, 2018), although some studies have suggested it might be related to photochemical oxidation of elemental Hg(0) in the tropopause (Cai and Chen, 2016; Chen et al., 2012a). Despite these uncertainties, Hg isotopes remain a powerful tool for tracing both the sources and redox pathways of Hg in rivers. Due to the very low Hg concentration (possibly less than $<$ 1 ng/L) in natural water which was a great challenge to the routine Hg isotope analysis, previous studies primarily focused on the sources and reactions affecting Hg in contaminated rivers using the isotope approach. Understanding Hg isotopes in large rivers may provide critical insight to Hg cycling in rivers and potentially the contribution of Hg from rivers to global ocean ecosystems.

In this study, we report the Hg isotope compositions of dissolved load in surface water, spring water, groundwater, rainwater, wastewater, rock, leaf litter, soil and $PM_{2.5}$ from the whole Pearl River Basin (PRB), the second largest river in China with a length of 2240 km. Located in a subtropical zone, the Pearl River originates from the Maxiong Mountain of Qujing City in Yunnan Province and flows through seven provinces in southern China and ends into the South China Sea. It has an average annual precipitation of 1470 mm and an average annual runoff of 3.2×10^{11} m^3, with a drainage basin estimated to be 4.5×10^5 km^2 (Liu et al., 2017a; Zhen et al., 2016). As an important water resource for industrial and domestic uses in Pearl River Delta (PRD), the most densely industrialized and urbanized region in China, the Pearl River is seriously polluted by industrial activities and domestic sewage (Liu et al., 2011, 2012; Zhen et al., 2016). Despite numerous studies have been conducted for Hg content, speciation and bioavailability in various materials from the PRD, such as sediments (Liu et al., 2011; Shao et al., 2011; Shi et al., 2010), soils and vegetables (Chen et al., 2012b; Shao et al., 2013), aquatic organisms (Shao et al., 2011, 2013) and river water (Liu et al., 2012; Zhen et al., 2016), the sources and processes affecting Hg in the Pearl River remain poorly understood. Because solar radiation, rainfall, water discharge and hydrodynamic condition would be obviously different at various flowrate stage and impact to different extent the sources and processes of Hg in rivers, samples collected both at flood and low water stages are investigated. Thus, the goals of this study are 1) to use Hg isotope compositions to identify the source of dissolved Hg in the Pearl River and its tributaries rivers 2) to determine the possibly key transformation processes that affect Hg transportation in the Pearl River.

2. Methods

2.1. Reagents and materials

Millipore-Q water (18.2 MΩ cm) and analytical grade reagents (HCl, HNO_3, H_2SO_4, $NH_2OH{\cdot}HCl$, $SnCl_2$, KBr, $KBrO_3$, L-cysteine) from both Sinopharm Chemical Reagent Co., Ltd (China) and Sigma-Aldrich (USA) were used throughout the experiment. The Hg standard solutions NIST SRM 3133 and NIST SRM 3177 were used as Hg isotope reference materials. The thallium solution NIST SRM 997 was used for instrumental mass bias correction (Blum and Bergquist, 2007; Chen et al., 2010). Most of the vessels were Teflon, glass or quartz made to minimize Hg sorption and cleaned with 1% BrCl, 15% HNO_3 before use, some of the PP (polypropylene) vessels were cleaned with 10% HNO_3 and rinsed with Milli-Q water before use. Both borosilicate glass vessels and quartz tubes were heated at 460 °C for 3 h to remove traces of Hg. The borosilicate glass column with a polypropylene reservoir and anion-exchange resin AG1-X4 (200–400 mesh, Bio-Rad®) was used for pre-concentration of dissolved Hg (Chen et al., 2010). The furnace quartz tube placed in two combustion tube furnaces were used for pre-concentration of Hg from rock, soil, leaf litter and $PM_{2.5}$ (Huang et al., 2015).

2.2. Sample collection and processing

Three sets of samples were collected in the PRB between May 2015 and December 2016. The locations of the sampling sites and detailed sampling information are shown in Fig. 1 and Tables S1, S2, S3. The first set of samples were surface water (n = 36) collected along the flow path of Pearl River from M1 (831 km) to M12 (2033 km) during the flood period of June 2015, the low water period of December 2015 and March 2016. The samples covered the mainstream such as Nanpan River (M1), Hongshuihe River (M2 to M4), Qianjiang River (M5 to M6), Xunjiang River (M7 to M8), Xijiang River (M9 to M12), and tributary rivers (Beipan River for T1, Liujiang River for T2, Yujiang River for T3, Guijiang River for T4, Hejiang River for T5, Beijiang River for T6). The second set of samples consisted of groundwater from carbonate rocks area (n = 2) and spring water from headwater of Pearl River (S0, n = 2) and rainwater in the urban area (Guangzhou, n = 3). The third set of samples were wastewaters which included untreated industrial wastewater (UIWW1), treated industrial wastewater (TIWW1-3), domestic wastewater (DW1) and mine wastewater (Pb and Zn, Mw1). Complementary samples (Table S3) consisted of carbonate rock (n = 2) and silicate rock (n = 2), leaf litter (n = 2), soil (n = 6) and $PM_{2.5}$ near electronic waste (E-waste) treatment plants (n = 1). The temperature and pH of all river water were measured *in situ* by a portable multi-parameter water quality meter (WTW-Multi 3430). Total suspended solids (TSS) in river water were analyzed in unfiltered water.

All collected water samples (4.9–9 L) were immediately filtered using a pre-cleaned Teflon filter system and mixed cellulose esters membrane filter (142 mm diameter, Millipore), which was commonly used for Hg isotopes studies in natural water systems (Chen et al., 2012a, 2016; Jiskra et al., 2017; Yuan et al., 2018). One study showed no Hg isotope fractionation when using different porosity of membrane (Jiskra et al., 2017). We used 0.22 μm porosity for filtration in order to eliminate the possible presence of colloidal Hg. For each sample, the first 200 mL of filtered water was discarded to avoid cross-contamination. The remaining filtered water was prepared as the following: i) 15 mL filtered water was stored in PP vessels for anions analysis and ii) 40 mL was stored in borosilicate glass bottles after acidification with three drops of H_2SO_4 for dissolved organic carbon (DOC) analysis. Blank of the filtration system was 13 pg Hg (n = 9). Then, a large volume of all filtered water was acidified in borosilicate glass bottles with HCl to 0.1 mol/L, digested with 0.5% (v/v) BrCl (0.2 mol/L) for about 12 h and stored at 4 °C before concentration and isotope analyses of total dissolved Hg. Major anions and DOC of filtered water were measured by ICS-90 (DIONEX) and High TOC II (Elementar). The Hg concentrations were measured by cold vapor atomic fluorescence spectrometry (CVAFS, measured with both Tekran 2500 and Brooks Rand), with a precision better than 5%.

2.3. Hg isotope measurement

2.3.1. Pre-concentration of Hg

The method used to pre-concentrate filtered water has been described in Chen et al. (2010). In brief, the chromatographic borosilicate glass column charged with 0.5 mL AG 1 × 4 resin was cleaned using 0.05% (w/v) L-cysteine in 4 mol/L HNO_3, 4 mol/L HNO_3 and Milli-Q water and then conditioned with 0.1 mol/L HCl. The HCl-acidified filtered water was first neutralized by a solution of 20% (w/v) $NH_2OH{\cdot}HCl$ to remove the excess BrCl and then loaded into the column with a flow rate of 3.5 mL/min. Before elution, the resin column was rinsed with 20 mL 0.1 mol/L HCl. We used 5 mL 0.05% (w/v) L-cysteine in 0.5 mol/L HNO_3 solution to elute the Hg, and double the concentrations for low water samples to ensure complete recovery of Hg. Finally, the eluted Hg of all filtered water was treated with BrCl to remove the excess of L-cysteine. The BrCl was neutralized by $NH_2OH{\cdot}HCl$ before the Hg isotope ratio measurements. The average procedural blank of this method was 75 pg (n = 8). NIST SRM 3133 was used as the procedural standard, which was processed the same as the samples and yielded a recovery of 98 ± 4% (SD, n = 9). The method used to pre-concentrate rock, leaf litter, soil and $PM_{2.5}$ has been described in Huang et al. (2015).

2.3.2. Hg isotope ratio analysis

Hg has seven stable isotopes, ^{196}Hg, ^{198}Hg, ^{199}Hg, ^{200}Hg, ^{201}Hg, ^{202}Hg and ^{204}Hg whose abundances are 0.16%, 10.04%, 16.94%, 23.14%, 13.17%, 29.73% and 6.83% in NIST SRM 3133 (Blum and Johnson, 2017). Hg isotope ratio measurements were performed on the MC-ICP-MS (Nu Instruments Ltd., UK) at the State Key Laboratory of Environmental Geochemistry, Institute of Geochemistry, Chinese Academy of Sciences, according to the previous methods (Blum and Bergquist, 2007; Chen et al., 2010; Yuan et al., 2018). In brief, the sample Hg solution (~0.5–3 ng/mL) was mixed with the $SnCl_2$ reagent using a peristaltic pump (0.75 mL/min) to produce the Hg(0) vapor. The Tl aerosol produced from an Aridus II desolvator was introduced together with the Hg(0) vapor into the plasma, which was used for mass bias correction. The Faraday cups were positioned to measure five Hg isotopes ^{198}Hg, ^{199}Hg, ^{200}Hg, ^{201}Hg, ^{202}Hg and two Tl isotopes ^{203}Tl, ^{205}Tl. ^{196}Hg and ^{204}Hg were not measured due to their low sensitivity. The instrumental mass bias was corrected by a combination of $^{205}Tl/^{203}Tl$ normalization and the sample-standard bracketing (SSB) method using NIST SRM 3133 as the bracketing standard. The Hg isotope composition is expressed by the delta notation ($\delta^x Hg$) in units of per mil (‰) and is defined below (Blum and Bergquist, 2007):

$$\delta^x Hg = \left[\frac{\left(\frac{^xHg}{^{198}Hg}\right)_{sample}}{\left(\frac{^xHg}{^{198}Hg}\right)_{std}} - 1 \right] \times 1000 \quad (1)$$

where x = 199, 200, 201, 202, "std" is the international standard NIST SRM 3133 Hg solution. The MDF is typically represented by $\delta^{202}Hg$. MIF is represented by "capital delta" ($\Delta^x Hg$, in ‰) defined following (Blum and Bergquist, 2007):

$$\Delta^{199}Hg = \delta^{199}Hg - 0.252 \times \delta^{202}Hg \quad (2)$$

$$\Delta^{200}Hg = \delta^{200}Hg - 0.502 \times \delta^{202}Hg \quad (3)$$

$$\Delta^{201}Hg = \delta^{201}Hg - 0.752 \times \delta^{202}Hg \quad (4)$$

NIST SRM 3177 Hg standard solution was measured in each analytical session to monitor the performance of the instrument. Long-term measurement of NIST SRM 3177 gave a mean $\delta^{202}Hg$ value of −0.57 ± 0.10‰ (2SD, n = 52) which is consistent with the values reported previously (Baptista-Salazar et al., 2018; Chen et al., 2016; Wang et al., 2015; Yuan et al., 2018). The 2SD of Hg isotope ratios in NIST SRM 3177 Hg standard solution ($\delta^{202}Hg$, $\Delta^{199}Hg$, $\Delta^{200}Hg$ and $\Delta^{201}Hg$ were 0.10‰, 0.06‰, 0.04‰ and 0.06‰) are reported as the typical analytic uncertainties of our most samples. The 2SD of Hg isotope ratios in most rock, leaf litter and soil are calculated by multiple measurements.

3. Results

The Hg concentrations and isotope compositions of all dissolved load in surface river water, natural and anthropogenic samples in PRB are listed in Tables S1, S2, S3 along with other parameters (T, pH, DOC, Cl^-, TSS and monthly discharge).

3.1. Geochemical characteristics of surface water

Surface water temperature ranged from 12 °C to 30 °C, with an average value of 27 °C and 17 °C during the flood and low water periods respectively. The surface water sampled at two periods are slightly alkaline with a pH ranging from 7.22 to 8.57 (the lowest pH at

downstream during two periods, Fig. S1a), while pH of most surface water sampled at flood water period are slightly lower. The TSS of surface water showed large variations ranging from 2.1 to 75.3 mg/L, with higher values during flood water period. TSS values of our samples are lower than the global average riverine level of 150 mg/L (Zheng et al., 2010). The DOC concentrations in all surface water varied from 0.73 to 23.07 mg/L with an average value of 3.69 ± 10.09 mg/L (2SD, n = 38, Fig. S1b), which is similar to the global natural river values (2–25 mg/L) (Zheng et al., 2010). The Cl^- concentrations in all surface water ranged from 0.87 to 8.71 mg/L with a mean value of 3.23 ± 3.30 mg/L (2SD, n = 38, Fig. S1c). It is worth noting that most DOC and Cl^- concentrations in flood water samples are higher than the one in low water samples. In average 80% of the annual rainfall occurs during wet season (Zhao et al., 2017), and the monthly discharge during flood water period are obviously higher than during low water period. Thus, the higher DOC and Cl^- concentrations in flood water may be caused by rainfall-induced soil erosion. We also note that DOC and Cl^- display slightly higher values at downstream during flood water period, which may reflect significant anthropogenic input via heavy rainfall or surface runoff leaching.

3.2. Hg concentrations and isotope compositions in surface river water

The dissolved Hg concentrations (Hg_d) in surface water for both flood water and low water samples ranged from 0.45 to 2.44 ng/L with a mean value of 1.20 ± 1.10 ng/L (2SD, n = 38, Table S1) in the Pearl River and its tributaries. The average Hg concentration in the human-impacted Pearl River is thus, lower than i) the Chinese drinking water value of 50 ng/L (Zhao et al., 2017), ii) new aquatic environmental total Hg quality standards limited at 70 ng/L (Tavares et al., 2016) and iii) the Hg levels in worldwide rivers impacted by mining and heavily industrialized and polymetallic pollution (Biber et al., 2015; Demers et al., 2018; Hissler and Probst, 2006; Kocman et al., 2011; Leitch et al., 2007; Washburn et al., 2017, 2018). However, the concentration is similar to the global unpolluted or agricultural and urban rivers (Lyons et al., 2006; Schuster et al., 2011; Wang et al., 2013; Zhao et al., 2017; Zheng et al., 2010). More specifically, flood water samples (from 0.58 (T3) to 2.44 ng/L (M10), mean = 1.60 ± 0.90 ng/L, 2SD, n = 19) exhibit a concentration of dissolved Hg twice higher than the low water samples (from 0.45 (T2) to 1.42 ng/L (M11), mean = 0.79 ± 0.55 ng/L, 2SD, n = 19, Fig. 2a), suggesting that flooding results in net Hg input to river. Besides, it is also worth noting that Hg_d in the surface water at the downstream are higher than other reaches (Fig. 2a).

Large variations are observed for $\delta^{202}Hg$ (−2.89‰ to −0.57‰, average −1.30 ± 1.02‰, 2SD, n = 38) and $\Delta^{199}Hg$ (−2.25‰ to 0.57‰, average 0.16 ± 1.05‰, 2SD, n = 38) in dissolved load. $\Delta^{201}Hg$ is similar and linearly correlated with $\Delta^{199}Hg$, thus in the following we will not discuss $\Delta^{201}Hg$ separately. $\Delta^{200}Hg$ values are mostly positive (−0.05‰–0.52‰), with a mean value of 0.08 ± 0.22‰ (2SD, n = 38, Table S1). Headwater obviously shows much lower $\delta^{202}Hg$ (down to −2.89‰), but similar $\Delta^{199}Hg$. Most dissolved loads are characterized by positive $\Delta^{199}Hg$ (0.10‰–0.57‰, average 0.30 ± 0.22‰, 2SD, n = 35) and negligible $\Delta^{200}Hg$ (average 0.05 ± 0.12‰, 2SD, n = 35) (Fig. 2b, c, 2d). Only three flood water samples at downstream (the mainstream M10, M11 and the tributary T6) displayed negative $\Delta^{199}Hg$ ranging from −2.25‰ to −0.76‰ and positive $\Delta^{200}Hg$ varying from 0.23‰ to 0.52‰ (Fig. 2c and d). Excluding these three samples, the mean values of $\delta^{202}Hg$ and $\Delta^{199}Hg$ in low water samples ($\delta^{202}Hg_{low}$ = −1.56 ± 1.06‰; $\Delta^{199}Hg_{low}$ = 0.36 ± 0.19‰, 2SD, n = 19) are more negative and positive than those in flood water samples ($\delta^{202}Hg_{flood}$ = −1.10 ± 0.70‰; $\Delta^{199}Hg_{flood}$ = 0.22 ± 0.14‰, 2SD, n = 16) respectively. The mean values of $\Delta^{200}Hg$ are similar between the two periods and close to 0‰. The isotope compositions of the dissolved Hg in surface water are quite different from contaminated rivers in the Northern Hemisphere which were characterized by higher $\delta^{202}Hg$ (−0.27 ± 0.99‰, 2SD, n = 63) and lower $\Delta^{199}Hg$ (0.06 ± 0.22‰, 2SD, n = 63) (Demers et al., 2018; Foucher et al., 2013; Washburn et al., 2017, 2018). Furthermore, $\delta^{202}Hg$ in surface water undergo wide variations along the flow path, but $\Delta^{199}Hg$ and $\Delta^{200}Hg$ display a relatively narrow range (except for three surface water with negative $\Delta^{199}Hg$ and more positive $\Delta^{200}Hg$, and $\Delta^{199}Hg$ of river water for M3 (1032 km) in low water period, Fig. 2b, c, 2d).

3.3. Hg concentrations and isotope compositions in natural water and wastewater

The Hg concentrations and isotope compositions of natural water and wastewater are reported in Table S2. The three precipitation samples collected at Guangzhou, China, display higher concentrations than surface water (1.75–3.55 ng/L vs 0.45–2.44 ng/L respectively). The groundwater collected from carbonate rocks area is characterized by Hg concentration ranging from 0.51 to 1.86 ng/L. In contrast, the average Hg concentrations for untreated industrial wastewater (UIWW1), treated industrial wastewater (TIWW1-3), domestic wastewater (DW1) and mine (Pb and Zn) wastewater (Mw1) are 1.96 ng/L, 1.65 ng/L (0.97–2.05 ng/L), 3.01 ng/L, 3.08 ng/L respectively. The Hg_d of most wastewater is higher than the surface water.

Rainwater from Guangzhou exhibited slightly negative $\delta^{202}Hg$ (−0.57 ± 0.70‰) and positive $\Delta^{199}Hg$ (0.42 ± 0.23‰) and slightly positive $\Delta^{200}Hg$ (0.17 ± 0.16‰) (2SD, n = 3). These Hg isotope compositions are consistent with the results reported previously (Wang et al., 2015; Yuan et al., 2018). The groundwater shows similar $\delta^{202}Hg$ (−0.96‰ and −0.58‰), and lower $\Delta^{199}Hg$ (0.08‰ and 0.13‰, n = 2). UIWW1 and TIWW1-3 are characterized by $\delta^{202}Hg$ of −1.58‰ to −0.86‰ and $\Delta^{199}Hg$ of 0.06‰ to 0.43‰ respectively ($\delta^{202}Hg$ = −1.19 ± 0.75‰, $\Delta^{199}Hg$ = 0.26 ± 0.34‰, 2SD, n = 4). The DW1 and Mw1 have more negative $\delta^{202}Hg$ of −2.48‰, −1.94‰ and positive $\Delta^{199}Hg$ of 0.34‰, 0.17‰ respectively. Groundwater and all wastewater display $\Delta^{200}Hg$ close to 0‰. The Hg isotope compositions of all wastewater are not significantly different from those of the river water ($\delta^{202}Hg$: $p = 0.32 > 0.05$; $\Delta^{199}Hg$: $p = 0.64 > 0.05$), probably due to the large variations of Hg isotope compositions of river water.

3.4. Hg concentrations and isotope compositions in watershed samples

The Hg concentrations and isotope compositions of watershed samples are reported in Table S3. The Hg concentrations in carbonate rock (n = 2) and silicate rock (n = 2) from the PRB are very low from 2 to 30 ng/g, while Hg concentration varying from 67 to 1075 ng/g was measured in soil (n = 6) from the PRB. Besides, the Hg concentration of leaf litter (n = 2) varied from 250 to 504 ng/g. Both silicate rock and carbonate rock are characterized by negative $\delta^{202}Hg$ varying from −2.99‰ to −1.75‰ and −1.29‰ to −0.37‰ respectively with both no significant Hg odd-MIF ($\Delta^{199}Hg$ ranging from 0.00‰ to 0.05‰ and −0.06‰ to −0.01‰ respectively). These signatures are consistent with the Hg isotope compositions reported for other rocks ($\delta^{202}Hg$: −2.68‰ to 1.61‰; $\Delta^{199}Hg$: −0.46‰ to 0.34‰) (Blum and Johnson, 2017; Blum et al., 2014). Besides, soil exhibited negative $\delta^{202}Hg$ varying from −1.70‰ to −0.83‰ and negative $\Delta^{199}Hg$ ranging from −0.58‰ to −0.01‰. This is agreement with soil data reported previously (e.g., $\delta^{202}Hg$ varying from −2.63‰ to 0.15‰, and $\Delta^{199}Hg$ varying from −0.56‰ to 0.07‰) (Blum et al., 2014; Jiskra et al., 2015, 2017; Zhang et al., 2013; Zheng et al., 2016). Leaf litters exhibit more negative $\delta^{202}Hg$ (−2.67‰ to −2.07‰) and $\Delta^{199}Hg$ values (−0.34‰ to −0.14‰) which are also consistent with other studies ($\delta^{202}Hg$: −3.28‰ to 1.50‰, and $\Delta^{199}Hg$: −1.58‰ to 0.33‰) (Blum et al., 2014). All samples are characterized by $\Delta^{200}Hg$ close to zero.

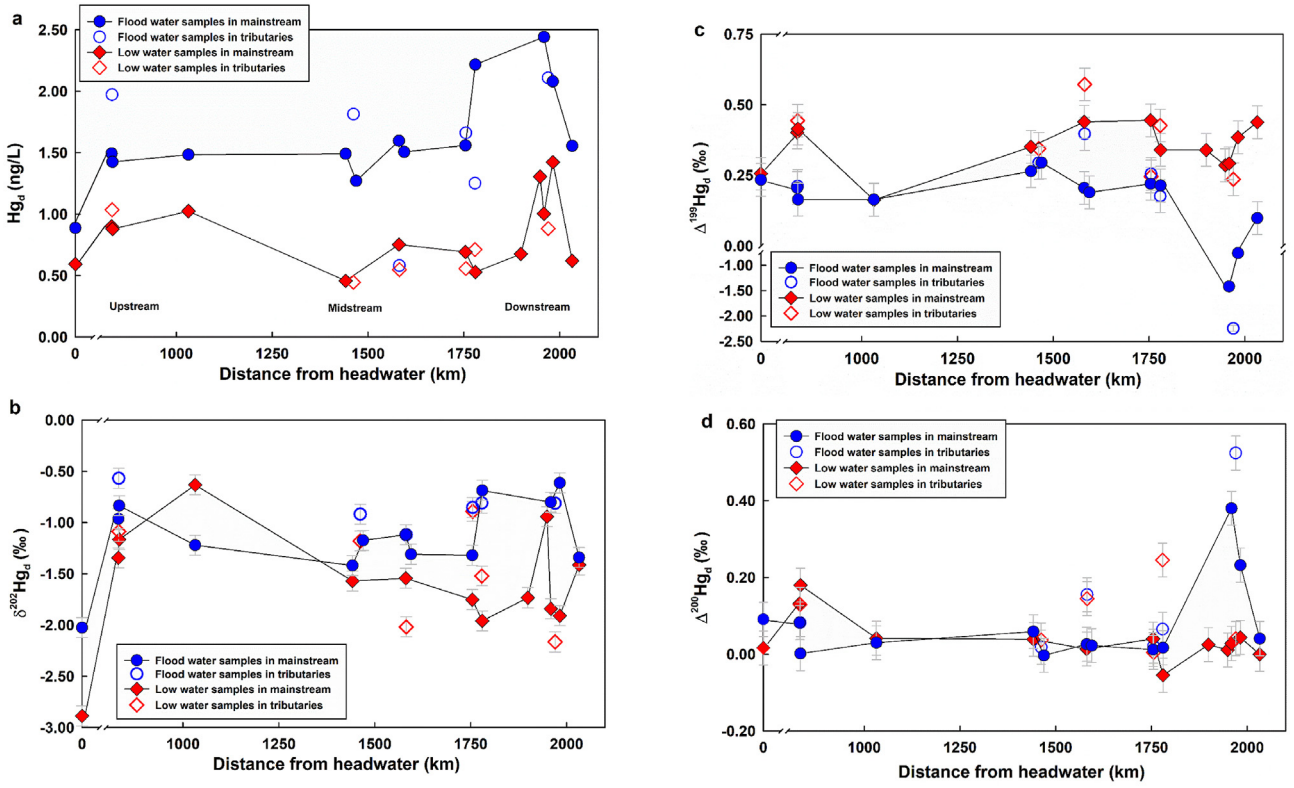

Fig. 2. Variations of dissolved Hg concentrations (Hg_d), $\delta^{202}Hg_d$, $\Delta^{199}Hg_d$ and $\Delta^{200}Hg_d$ for dissolved load in surface water with sampling distance from the headwater. The analytical uncertainty of Hg isotope measurements (2SD) is presented in method.

4. Discussion

4.1. Effect of tributaries on mainstream Hg budget

As shown in Fig. 2, dissolved Hg concentrations (Hg_d) and Hg isotope compositions of the mainstream could be influenced by the input of tributaries. The effect of Hg isotope compositions from the tributaries input on the mainstream (predominantly via the flux of dissolved Hg) is estimated following:

$$\delta^{202}Hg_{Mi,Theo} \times Hg_{Mi,d} \times F_{Mi} = (\delta^{202}Hg_{Mi-1} \times Hg_{Mi-1,\,d} \times F_{Mi-1}) + (\delta^{202}Hg_{Tj} \times Hg_{Tj,\,d} \times F_{Tj}) \quad (5)$$

$$\Delta^{199}Hg_{Mi,Theo} \times Hg_{Mi,d} \times F_{Mi} = (\Delta^{199}Hg_{Mi-1} \times Hg_{Mi-1,\,d} \times F_{Mi-1}) + (\Delta^{199}Hg_{Tj} \times Hg_{Tj,\,d} \times F_{Tj}) \quad (6)$$

where M*i* and M*i-1* are the *i*th and *i*-1st sampling sites of mainstream nearby *j*th sampling site of tributary (T*j*) and F is water flow (m^3/s). $Hg_{Mi,\,d}$, $Hg_{Mi-1,\,d}$ and $Hg_{Tj,\,d}$ refer to dissolved Hg concentrations at the *i*th, *i*-1st sampling sites of mainstream and *j*th sampling site of tributary respectively. $\delta^{202}Hg_{Mi,Theo}$ and $\Delta^{199}Hg_{Mi,Theo}$ are the theoretical Hg isotope compositions of dissolved phase for mainstream (M*i*) after mixing between the mainstream (M*i-1*) and the near tributary (T*j*). Theoretical Hg isotope compositions of dissolved load at M5 (mixing by M4 and T2) and M11 (mixing by M10 and T6) during flood water period, and the theoretical Hg isotope compositions of dissolved load at M11 during low water period are calculated. During flood water period, the theoretical $\delta^{202}Hg$ and $\Delta^{199}Hg$ of dissolved load would be −1.63‰ and 0.43‰ respectively for M5 (observed values of −1.17‰ and 0.30‰), −1.11‰ and −2.09‰ respectively for M11 (observed values of −0.61‰ and −0.76‰), while during low water period, theoretical $\delta^{202}Hg$ and $\Delta^{199}Hg$ of dissolved load would be −1.58‰ and 0.22‰ respectively for M11 (observed values of −1.91‰ and 0.38‰). Thus, theoretical $\delta^{202}Hg$ and $\Delta^{199}Hg$ in the dissolved load after mixing by mainstream and tributary are different from the observed values. This suggests that Hg isotope compositions of mainstreams may be influenced by other factors such as processes occurring within the river or the input of additional Hg sources.

4.2. Possible effects of in_situ riverine processes

Hg isotope compositions in natural water systems may be affected by physical and chemical processes and by the input of Hg from additional sources. Hg in natural water can undergo various processes, including microbial processes such as reduction of Hg(II) (Kritee et al., 2007), degradation and formation of MeHg (Kritee et al., 2009; Rodríguez-González et al., 2009), abiotic processes such as adsorption and precipitation of Hg(II) (Foucher et al., 2013; Jiskra et al., 2012; Wiederhold et al., 2010), photo-reduction of Hg(II) and MeHg (Bergquist and Blum, 2007; Zheng and Hintelmann, 2009, 2010a), dark reduction and methylation of Hg(II) (Malinovsky and Vanhaecke, 2011; Zheng and Hintelmann, 2010b), volatilization and aqueous oxidation of Hg(0) (Zheng et al., 2007, 2018). All these processes could produce Hg isotope fractionation. Below we discuss how these processes could affect the Hg isotope compositions in river water and we will try to identify which processes are most likely the dominant one in the Pearl River system.

Note that Hg(0) photo-oxidation is not discussed in this study, because Hg(0) in rivers accounts for only a small portion (~10%–30%) (Leopold et al., 2010). Moreover, isotope fractionation during photo-oxidation of dissolved Hg(0) is unknown. The processes about MeHg are also not considered because the MeHg concentration in dissolved load is very low (0.14 ± 0.05 ng/L) and only accounts for < 1% of total mercury concentration (Liu et al., 2012). Thus, MeHg formation and degradation are unlikely responsible for the variations of the Hg isotope compositions in PRB.

4.2.1. Partitioning effects on Hg isotope fractionation

Previous studies have reported that equilibrium and kinetic processes may influence Hg partitioning between dissolved and particulate phases. The experiments on Hg(II) adsorption and precipitation on minerals and organic matter ($\delta^{202}Hg_{p\text{-}d}$) have showed that heavy Hg isotopes prefer to be enriched in the Hg(II) solution (e.g., $\delta^{202}Hg_{p\text{-}d}$ up to −0.67‰) (Demers et al., 2018; Foucher et al., 2013; Jiskra et al., 2012; Wiederhold et al., 2010). In this study, the offset between $\delta^{202}Hg$ values of dissolved and suspended phases ($\delta^{202}Hg_{p\text{-}d}$ see Supplementary Materials) is mainly negative during the flood water period ($\delta^{202}Hg_{p\text{-}d}$ ranging from −1.53‰ to 0.03‰) while the $\delta^{202}Hg_{p\text{-}d}$ during the low water period is mainly positive (−0.43‰ to 1.50‰, Fig. S2). If the $\delta^{202}Hg$ values of dissolved and suspended phases were influenced by fractionation processes during partitioning, $\delta^{202}Hg_{p\text{-}d}$ offset would appear to correlate with some geochemical parameters (e.g., pH, Cl^-, DOC, Hg_d, TSS etc.). Previous studies have reported that Hg may be increasingly desorbed from suspended phase into dissolved phase with increasing DOC and Cl^- concentrations and pH (> 7.5, especially for pH higher than 8). Moreover, the formation of Hg–Cl complexes is important only at low pH (< 7) or high Cl^- concentration (> 12 mg/L) (Hissler and Probst, 2006; Kocman et al., 2011; Lyons et al., 2006) which is at odds with our measurement with higher pH (7.22–8.57) and lower Cl^- concentration (0.87–8.71 mg/L). Thus, we focus on the relationship among $\delta^{202}Hg_{p\text{-}d}$ offset, pH, DOC, Hg_d and TSS.

The $\delta^{202}Hg_{p\text{-}d}$ offset between dissolved and suspended phases displays slightly positive correlation with pH ($R^2 = 0.19$, $p < 0.01$, Fig. S2a) and negative correlation with DOC ($R^2 = 0.40$, $p < 0.01$, Fig. S2b). Moreover, the $\delta^{202}Hg_{p\text{-}d}$ offset shows significantly negative correlation with dissolved Hg concentrations (Hg_d, $R^2 = 0.56$, $p < 0.01$, Fig. S2c). As discussed above, if more suspended Hg entered dissolved phase at higher pH and DOC and Hg_d, this may generate $\delta^{202}Hg_{p\text{-}d}$ offset closer to 0‰. But we observe large variations of $\delta^{202}Hg_{p\text{-}d}$ offset with increased pH, DOC and Hg_d during the partitioning (Figs. S2a, S2b, S2c). Moreover, the $\delta^{202}Hg_{p\text{-}d}$ offset displays no significant relationship with TSS, especially during flood water period (Fig. S2d). Some studies also suggested that dissolved and particulate phases in a dynamic flowing river system are unlikely to reach thermodynamic equilibrium due to different concentrations of Hg complexing ligands or the loss of dissolved Hg to the atmosphere (Foucher et al., 2013; Leitch et al., 2007). These arguments suggest that Hg isotopes in surface water may not be primarily controlled by fractionation processes during partitioning.

4.2.2. The effects of Hg reduction on its isotope compositions

The river water samples in this study are plotted along a slope of 1.09 in a $\Delta^{199}Hg/\Delta^{201}Hg$ diagram (excluding M10, M11 and T6 in flood water period treated as outliers, Fig. 4), suggesting that Hg in river water is mainly controlled by Hg(II) photochemical reduction that is characterized by a slope of ~1 (Bergquist and Blum, 2007; Zheng and Hintelmann, 2009). Abiotic dark reduction of Hg(II) would be not the main process, because this process is characterized by a slope of 1.5–1.6 (Zheng and Hintelmann, 2010b).

Photochemical reduction of Hg(II) would increase $\delta^{202}Hg$ and $\Delta^{199}Hg$ or decrease $\Delta^{199}Hg$ in river water, and the subsequent volatilization of product Hg(0) would further increase $\delta^{202}Hg$ (Demers et al., 2018; Zheng et al., 2007; Zheng and Hintelmann, 2009, 2010a). However, the river water samples exhibit either a decrease or little change in $\delta^{202}Hg$ values in the overall river systems with no inputs of large tributaries along the flow path (e.g., dissolved Hg from M2 (833 km) to M4 (1442 km), M7 (1594 km) to M8 (1754 km), M9 (1780 km) to M10 (1959 km) and M11 (1982 km) to M12 (2033 km) at flood water stage; dissolved Hg from M3 (1032 km) to M4 (1442 km) and M9-A2 (1949 km) to M10 (1959 km) at low water stage, Fig. S3b). Some parts of the river with no inputs of large tributaries display increasing $\delta^{202}Hg$ and decreasing $\Delta^{199}Hg$ along the flow path, which may be explained by photochemical reduction of Hg(II) from sulfur bearing ligands (e.g., dissolved Hg from M5 (1469 km) to M6 (1581 km) during flood water period; dissolved Hg from M2 (833 km) to M3 (1032 km), M9 (1780 km) to M9-A2 (1949 km) during low water period, Figs. S3b and S3c) (Zheng and Hintelmann, 2010a). However, photo-reduction should result in a loss of dissolved Hg, while Hg_d in these river waters exhibit increasing trends during the two periods (Fig. S3a). Only river waters from M11 to M12 in low water period display an increasing trend in $\delta^{202}Hg$ from −1.91‰ to −1.41‰ and $\Delta^{199}Hg$ from 0.38‰ to 0.44‰, and decreasing trend in Hg_d from 1.42 to 0.62 ng/L. This may be influenced by photochemical reduction of Hg(II). Therefore, most of our data cannot be explained through photochemical reduction of Hg (II) alone.

It is worth noting that the three surface water samples during flood water period (M10, M11 and T6) are characterized by negative $\Delta^{199}Hg$ values varying from −2.25‰ to −0.76‰ (Fig. 2c). These are the first negative $\Delta^{199}Hg$ values reported in surface river water. The ratios of $\Delta^{199}Hg/\Delta^{201}Hg$ for these water samples range from 1.59 to 1.76. These negative $\Delta^{199}Hg$ values are unlikely caused by photo-oxidation of gaseous Hg(0), because the oxidation of Hg(0) by photochemically generated Cl atoms is characterized by a slope of 1.89 in a $\Delta^{199}Hg/\Delta^{201}Hg$ diagram (Sun et al., 2016). Because the three surface water samples with such negative odd-MIF are closely located, we suspect inputs of additional local Hg source to river characterized by negative odd-MIF.

4.3. Sources of Hg in surface river water

Previous studies have reported that Hg in rivers might derive from atmospheric precipitation, surface runoff, soil leaching, erosion and Hg-containing effluents (urban and combustion and industrial discharges) (Kocman et al., 2017; Wang et al., 2004). Here, we try to use Hg isotopes to identify the Hg sources of dissolved load in surface water in Pearl River.

4.3.1. Contribution of atmospheric precipitation

Previous literatures have reported that 90% of the Hg in surface water result from atmospheric deposition, with atmospheric precipitation being one of the main sources (Chen et al., 2016; Leopold et al., 2010; Obrist et al., 2018). The PRB is controlled by a humid subtropical climate with abundant annual rainfall ranging from 1000 to 2000 mm (Liu et al., 2017a). The upstream of PRB is dominated by karst landforms, facilitating the transport of atmospheric precipitation to terrestrial system to river basin due to the thin soil layer and the well distributed rock structure.

In this study, the Hg_d in flood water samples are higher than low water samples (Fig. 2a). Although some studies have reported that dissolved Hg concentrations in precipitation from Guizhou, China during the dry season (low water period) were higher than during the wet season (flood water period) (Guo et al., 2008; Wang et al., 2015; Yuan et al., 2018), the low rainfall intensity during dry season may still result in less Hg input via precipitation during low water period. The precipitation during the wet season accounts for an average 80% of the annual rainfall (Zhao et al., 2017) and Hg_d in surface water and monthly discharge show a positive correlation ($R^2 = 0.44$, $p < 0.01$, Fig. S4). This may cause higher Hg deposition fluxes and watershed Hg input during flood period. Interestingly, the Hg_d of the surface water in PRB is lower than the one reported for the precipitation. This may be caused by i) a time offset between the deposition of Hg to terrestrial watersheds and its transport to streams or ii) a possible loss of Hg during transport, for example by surface sorption (Stoken et al., 2016).

The Hg isotope compositions of flood ($\delta^{202}Hg = -1.10 \pm 0.70$‰, $\Delta^{199}Hg = 0.22 \pm 0.14$‰, $\Delta^{200}Hg = 0.05 \pm 0.08$‰, 2SD, n = 16) and low ($\delta^{202}Hg = -1.56 \pm 1.06$‰, $\Delta^{199}Hg = 0.36 \pm 0.19$‰, $\Delta^{200}Hg = 0.06 \pm 0.15$‰, 2SD, n = 19) water samples are similar to those reported for atmospheric precipitation during wet and dry seasons in both Guiyang and Guangzhou, China ($\delta^{202}Hg_{wet} = -1.00 \pm 0.73$‰, $\Delta^{199}Hg_{wet} = 0.40 \pm 0.30$‰,

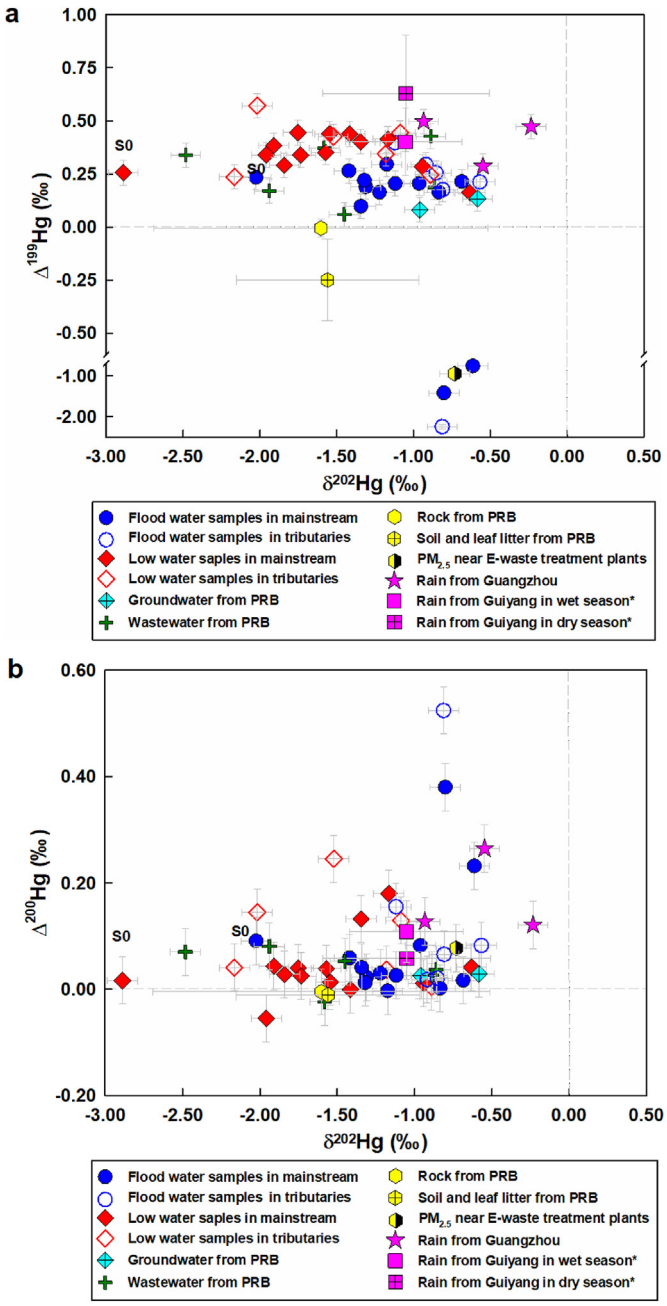

Fig. 3. Hg isotope compositions (δ^{202}Hg vs. Δ^{199}Hg and δ^{202}Hg vs. Δ^{200}Hg) of samples from Pearl River Basin (PRB). The analytical uncertainty of Hg isotope measurements (2SD) is presented in method. Error bars are mean ± 1SD for the rock, soil and leaf litter. *Data from Guiyang precipitation reported in the previous studies (mean ± 1SD) (Wang et al., 2015; Yuan et al., 2018).

$\Delta^{200}Hg_{wet}$ = 0.12 ± 0.14‰, 2SD, n = 13; $\delta^{202}Hg_{dry}$ = −1.01 ± 1.12‰, $\Delta^{199}Hg_{dry}$ = 0.62 ± 0.54‰, $\Delta^{200}Hg_{dry}$ = 0.06 ± 0.08‰, 2SD, n = 20) (Table S2, Fig. 3) (Wang et al., 2015; Yuan et al., 2018). Together with the fact that both dissolved Hg in surface water (excluding flood water samples of M10, M11 and T6 treated as outliers) and the precipitation show a similar slope of 1 in a $\Delta^{199}Hg/\Delta^{201}Hg$ diagram (Fig. 4), we suggest a significant contribution from atmospheric precipitation to river water. Moreover, the positive Δ^{200}Hg values in the three surface waters (up to 0.52‰, Fig. 3b) also suggest the input of atmospheric precipitation. However, most Δ^{199}Hg and Δ^{200}Hg values of dissolved Hg in surface water during the two periods are lower than the atmospheric precipitation (Fig. 3), suggesting the presence of an additional Hg source with lower Δ^{199}Hg and Δ^{200}Hg.

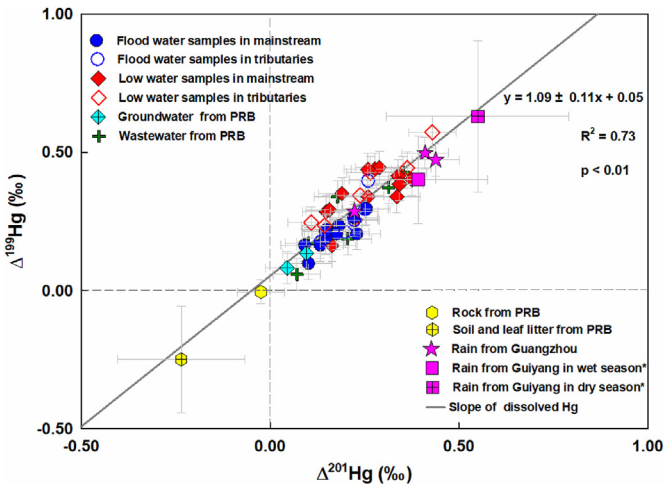

Fig. 4. Relationship between mass-independent fractionation (Δ^{201}Hg vs. Δ^{199}Hg) of samples from Pearl River Basin (PRB) (except for flood water samples of M10, M11 and T6 treated as outliers). The analytical uncertainty of Hg isotope measurements (2SD) is presented in method. Error bars are mean ± 1SD for the rock, soil and leaf litter. *Data from Guiyang precipitation reported in the previous studies (mean ± 1SD) (Wang et al., 2015; Yuan et al., 2018).

4.3.2. *Contribution of Hg by the watershed*

The PRB locates in a subtropical area with abundant vegetation where the forest coverage rate in the watershed is about 28%. The bedrock of the basin is mainly composed of carbonate and silicate rocks while various types of soil are also reported (e.g., red soil, lateritic soil, yellow soil, mountain meadow soil and lime soil, etc.). Moreover, numerous studies have reported that these materials showed large variations of Hg concentrations and isotope compositions, and with lower Δ^{199}Hg and near zero Δ^{200}Hg (Blum et al., 2014; Jiskra et al., 2015; Zheng et al., 2016). Therefore, the contribution of Hg in the watershed cannot be ignored. Below we will discuss potential sources from the watershed.

Silicate and carbonate rocks collected from PRB displayed negative δ^{202}Hg, without significant MIF (δ^{202}Hg = −1.60 ± 2.18‰, Δ^{199}Hg = 0.00 ± 0.09‰, Δ^{200}Hg = 0.01 ± 0.06‰, 2SD, n = 4, Fig. 3, Table S3). Silicate rocks are characterized by lower δ^{202}Hg values than carbonate rocks. Although rocks are characterized by a low Δ^{199}Hg and Δ^{200}Hg close to 0‰, the δ^{202}Hg of dissolved Hg from the upstream areas that are mainly composed of carbonate rocks are similar with the downstream areas that are mainly composed of silicate rocks. These suggest that bedrocks are unlikely the main controlling factors for the dissolved Hg isotope compositions in Pearl River.

Although leaf litter from PRB had negative δ^{202}Hg and Δ^{199}Hg, and Δ^{200}Hg close to zero (δ^{202}Hg = −2.37 ± 0.85‰, Δ^{199}Hg = −0.24 ± 0.28‰, Δ^{200}Hg = 0.01 ± 0.03‰, 2SD, n = 2, Table S3), Hg in the vegetation can be incorporated into the soil through litters (Jiskra et al., 2015; Zhang et al., 2013; Zheng et al., 2016). Thus, erosion and transport of watershed soils could be another potential Hg source (Baptista-Salazar et al., 2017; Biber et al., 2015; Kocman et al., 2017; Leitch et al., 2007; Stoken et al., 2016; Wang et al., 2004). Soils in the basin are characterized by negative δ^{202}Hg and Δ^{199}Hg (δ^{202}Hg = −1.29 ± 0.66‰, Δ^{199}Hg = −0.25 ± 0.44‰, 2SD, n = 6, Table S3). Soils influenced by anthropogenic activities generally displayed negative δ^{202}Hg and negligible Δ^{199}Hg (Blum et al., 2014), while forest soils were characterized by lower δ^{202}Hg and Δ^{199}Hg (Jiskra et al., 2015, 2017; Woerndle et al., 2018; Zhang et al., 2013; Zheng et al., 2016). All reported soils displayed Δ^{200}Hg close to zero. Although no studies have reported Hg isotope fractionation

associated with soil weathering processes, experimental studies on dissolution adsorption and co-precipitation have suggested that these processes would not modify Δ^{199}Hg. Moreover, previous studies showed that Hg associated with natural organic matter from forest soils into runoff displayed negative Δ^{199}Hg values and Δ^{200}Hg close to zero, these are similar to those from the forest soils (Jiskra et al., 2015, 2017; Washburn et al., 2018; Woerndle et al., 2018). Thus, Hg released from soil weathering processes into the runoff would retain the Δ^{199}Hg and Δ^{200}Hg signatures of soils.

In this study, groundwaters is characterized by negative δ^{202}Hg value of −0.96‰ to −0.58‰, and positive Δ^{199}Hg value of 0.08‰–0.13‰ (n = 2). The spring water (S0, n = 2) displays more negative δ^{202}Hg (−2.89‰ to −2.02‰) which might be related to the different lithology of the watershed, and more positive Δ^{199}Hg (0.23‰–0.26‰). Neither groundwater nor spring water show significant Δ^{200}Hg (close to 0‰). Δ^{199}Hg and Δ^{200}Hg values in both groundwater and spring water are lower than those of precipitation. This suggests that Hg in groundwater and spring water may result from a mixing between atmospheric precipitation and soil weathering products. Therefore, soil weathering products may be the main controlling factors for dissolved Hg isotope compositions of surface water in PRB, which cause lower Δ^{199}Hg and Δ^{200}Hg in river water than in the precipitation (Figs. 3 and 4). Moreover, δ^{202}Hg reported in dissolved load during the flood water period are higher than the low water period which could be explained by a higher contribution from precipitation. Indeed, the contribution from the precipitation to the river water during the flood water period is expected to be higher than during the low water period, because 80% of the annual precipitation occurs during the wet season in PRB. Based on the above discussion, the Hg inputs from atmospheric precipitation and surface soil weathering are likely to be major sources of Hg in surface river water.

4.3.3. Anthropogenic sources of Hg

Wastewater. Local wastewater is unlikely an important source of Hg for surface water in Pearl River. During the recent years, the concentrations of aqueous Hg released from local industrial wastewater and municipal sewage in China decreased due to the regulation of the wastewater discharge by the Chinese government. Moreover, primary anthropogenic Hg emitted into atmosphere is still important with a Hg released to water and air ratio of 1:5 (Liu et al., 2017b). Although approximately 23 Mg Hg was released from municipal sewage into aquatic environments (river, lake) in 2015 (Liu et al., 2016), around 95% of the total Hg in the influent sewage was transferred into the sewage sludge which may lower the concentration of industrial wastewater (0.97–3.08 ng/L) (Liu et al., 2017b). This is consistent with Hg concentrations of wastewater in this study.

Moreover, dissolved Hg in surface water show no significant relationship with Zn, an element easily influenced by human activities (Chen et al., 2008). In addition, since 2009, industrial wastewater had decreased after enterprises with high wastewater discharge were shut down in the PRD region and the transfer of small-scale electroplating facilities from the PRD into the inland regions (Zhen et al., 2016). Moreover, the Hg isotope compositions of wastewater from PRB (δ^{202}Hg = −1.53 ± 1.25‰, Δ^{199}Hg = 0.26 ± 0.28‰, Δ^{200}Hg = 0.04 ± 0.07‰, 2SD, n = 6) are similar with those of the surface river water (Fig. 3). This suggests that industrial water may be primarily sourced from river water.

Electronic wastes as potential sources of Hg. Three water samples M10, M11 and T6 collected during the flood water period almost in the same area (Fig. 1) display abnormal Δ^{199}Hg (−1.47 ± 1.49‰, 2SD, n = 3), which cannot be explained by the contribution of sources (processes) discussed above. Coincidently, these samples were collected at locations near E-waste treatment plants (Gao et al., 2008). We collected also both $PM_{2.5}$ and soil samples near the E-waste treatment plants with δ^{202}Hg of −0.73‰ and −1.49‰ and Δ^{199}Hg of −0.95‰ and −0.36‰, respectively (Fig. 3, Table S3), and find that $PM_{2.5}$ shows similar δ^{202}Hg but much lower Δ^{199}Hg compared to most airborne particulate Hg reported so far (Blum et al., 2014; Huang et al., 2019; Xu et al., 2019). These values are similar to the surface water of M10, M11 and T6 during the flood water period, strongly suggesting the influence of electronic wastes. One study reported that compact fluorescent lamps (CFL) were characterized by distinct Hg isotope compositions. The negative Δ^{199}Hg down to −21.49‰ was observed in Hg trapped in glass, and rarely negative Δ^{201}Hg (mostly positive) down to −0.24‰ were reported for Hg vapor in lamp (Mead et al., 2013). Though the direct contribution of CFL cannot account for the abnormal odd-MIF due to the very different Δ^{199}Hg/Δ^{201}Hg ratio from our samples, a mixing with other E-waste material would be a possible cause. More systematic study is thus needed to well constrain the origin of unusual odd-MIF.

During the flood water period, deposition of atmospheric particle-bound Hg from the atmosphere into river is important (Guo et al., 2008). Large amounts of Hg released from electronic wastes could be deposited into the river through precipitation or leached by soils near E-waste treatment plants. Previous study has reported that particles in rainwater were characterized by a mean Δ^{199}Hg of 0.16‰ (Yuan et al., 2018). We suggest that negative Δ^{199}Hg of $PM_{2.5}$ near E-waste treatment plants could result from a mixing between atmospheric particles characterized by positive Δ^{199}Hg and electronic wastes input characterized by more negative Δ^{199}Hg. This implies that the incineration of electronic wastes may produce more negative Hg odd-MIF that could be finally brought into river.

5. Conclusions and implications

This study reports for the first time Hg isotope compositions in the Pearl River, a highly anthropogenic-influenced large river. All dissolved load measured during flood and low water periods are characterized by negative δ^{202}Hg, slightly positive Δ^{200}Hg, and mostly positive Δ^{199}Hg, which are similar to the Hg isotope compositions reported in the local atmospheric precipitation. The isotope compositions suggest that atmospheric precipitation is the major Hg source to surface water. Furthermore, some surface water samples display less positive or more negative odd-MIF than those in precipitation. We suggest that this could not be explained by in-river processes, but would rather indicate the influence of groundwater and spring water formed by the interaction between atmospheric precipitation and soils weathering in the watershed, which are important dissolved Hg sources in surface river water. Interestingly, extremely negative Δ^{199}Hg were found in three surface filtered water, for which we propose primarily a contribution from electronic wastes. Therefore, our study has potential implications for tracing Hg sources from electronic wastes, although more studies on Hg isotope compositions in electronic wastes are needed in the future. This study demonstrates that the use of Hg isotopes in complex freshwater ecosystems (especially large rivers) can give insights into both processes and potential Hg sources. It would also provide basic data to research the contribution of Hg from rivers to global ocean ecosystems.

CRediT authorship contribution statement

Yuanyuan Zhang: Conceptualization, Methodology, Software, Validation, Investigation, Writing - original draft. **Jiubin Chen:** Conceptualization, Resources, Data curation, Writing - review & editing, Supervision, Project administration, Funding acquisition. **Wang Zheng:** Writing - review & editing. **Ruoyu Sun:** Writing - review & editing. **Shengliu Yuan:** Software, Validation, Formal analysis, Investigation, Visualization. **Hongming Cai:** Validation, Formal analysis, Investigation, Visualization. **David Au Yang:** Writing - review & editing. **Wei Yuan:** Software, Formal analysis, Investigation, Visualization. **Mei Meng:** Writing - review & editing. **Zhongwei Wang:** Software, Formal analysis, Investigation, Visualization. **Yulong Liu:** Formal analysis, Investigation, Visualization. **Jianfeng Liu:** Formal

analysis, Investigation, Visualization.

Acknowledgements

This research was financially supported by National Natural Science Foundation of China (41561134017, 41625012, U1612442, 41830647, U1301231), “ten thousand talent” project of Ministry of Science and Technology of the People's Republic of China, “hundred talent” project of Guizhou Science and Technology Department.

Appendix A. Supplementary data

Supplementary data to this article can be found online at https://doi.org/10.1016/j.ecoenv.2020.110229.

References

Amos, H.M., Jacob, D.J., Kocman, D., Horowitz, H.M., Zhang, Y., Dutkiewicz, S., Horvat, M., Corbitt, E.S., Krabbenhoft, D.P., Sunderland, E.M., 2014. Global biogeochemical implications of mercury discharges from rivers and sediment burial. Environ. Sci. Technol. 48, 9514–9522.

Baptista-Salazar, C., Hintelmann, H., Biester, H., 2018. Distribution of mercury species and mercury isotope ratios in soils and river suspended matter of a mercury mining area. Environ. Sci. Proc. Imp. 20, 621–631.

Baptista-Salazar, C., Richard, J.-H., Horf, M., Rejc, M., Gosar, M., Biester, H., 2017. Grain-size dependence of mercury speciation in river suspended matter, sediments and soils in a mercury mining area at varying hydrological conditions. Appl. Geochem. 81, 132–142.

Beckers, F., Rinklebe, J., 2017. Cycling of mercury in the environment: sources, fate, and human health implications: a review. Crit. Rev. Environ. Sci. Technol. 47, 693–794.

Bergquist, B.A., Blum, J.D., 2007. Mass-dependent and-independent fractionation of Hg isotopes by photoreduction in aquatic systems. Science 318, 417–420.

Biber, K., Khan, S.D., Shah, M.T., 2015. The source and fate of sediment and mercury in Hunza River basin, Northern Areas, Pakistan. Hydrol. Process. 29, 579–587.

Blum, J.D., Bergquist, B.A., 2007. Reporting of variations in the natural isotopic composition of mercury. Anal. Bioanal. Chem. 388, 353–359.

Blum, J.D., Johnson, M.W., 2017. Recent developments in mercury stable isotope analysis. Rev. Mineral. Geochem. 82, 733–757.

Blum, J.D., Sherman, L.S., Johnson, M.W., 2014. Mercury isotopes in earth and environmental sciences. Annu. Rev. Earth Planet Sci. 42, 249–269.

Cai, H., Chen, J., 2016. Mass-independent fractionation of even mercury isotopes. Sci. Bull. 61, 116–124.

Carroll, R.W.H., Warwick, J., Heim, K., Bonzongo, J., Miller, J., Lyons, W., 2000. Simulation of mercury transport and fate in the Carson River, Nevada. Ecol. Model. 125, 255–278.

Chen, J., Gaillardet, J., Louvat, P., 2008. Zinc isotopes in the Seine River waters, France: a probe of anthropogenic contamination. Environ. Sci. Technol. 42, 6494–6501.

Chen, J., Hintelmann, H., Dimock, B., 2010. Chromatographic pre-concentration of Hg from dilute aqueous solutions for isotopic measurement by MC-ICP-MS. J. Anal. Atom. Spectr. 25, 1402–1409.

Chen, J., Hintelmann, H., Feng, X., Dimock, B., 2012a. Unusual fractionation of both odd and even mercury isotopes in precipitation from Peterborough, ON, Canada. Geochem. Cosmochim. Acta 90, 33–46.

Chen, J., Hintelmann, H., Zheng, W., Feng, X., Cai, H., Wang, Z., Yuan, S., Wang, Z., 2016. Isotopic evidence for distinct sources of mercury in lake waters and sediments. Chem. Geol. 426, 33–44.

Chen, L., Xu, Z., Ding, X., Zhang, W., Huang, Y., Fan, R., Sun, J., Liu, M., Qian, D., Feng, Y., 2012b. Spatial trend and pollution assessment of total mercury and methylmercury pollution in the Pearl River Delta soil, South China. Chemosphere 88, 612–619.

Demers, J.D., Blum, J.D., Brooks, S.C., Donovan, P.M., Riscassi, A.L., Miller, C.L., Zheng, W., Gu, B., 2018. Hg isotopes reveal in-stream processing and legacy inputs in east fork poplar creek, oak ridge, Tennessee, USA. Environ. Sci. Proc. Imp. 20, 686–707.

Donovan, P.M., Blum, J.D., Singer, M.B., Marvin-DiPasquale, M., Tsui, M.T., 2016. Isotopic composition of inorganic mercury and methylmercury downstream of a historical gold mining region. Environ. Sci. Technol. 50, 1691–1702.

Driscoll, C.T., Mason, R.P., Chan, H.M., Jacob, D.J., Pirrone, N., 2013. Mercury as a global pollutant: sources, pathways, and effects. Environ. Sci. Technol. 47, 4967–4983.

Emmerton, C.A., Graydon, J.A., Gareis, J.A., St Louis, V.L., Lesack, L.F., Banack, J.K., Hicks, F., Nafziger, J., 2013. Mercury export to the Arctic ocean from the Mackenzie river, Canada. Environ. Sci. Technol. 47, 7644–7654.

Estrade, N., Carignan, J., Sonke, J.E., Donard, O.F., 2009. Mercury isotope fractionation during liquid–vapor evaporation experiments. Geochem. Cosmochim. Acta 73, 2693–2711.

Foucher, D., Hintelmann, H., Al, T.A., MacQuarrie, K.T., 2013. Mercury isotope fractionation in waters and sediments of the Murray Brook mine watershed (New Brunswick, Canada): tracing mercury contamination and transformation. Chem. Geol. 336, 87–95.

Gao, B., Sun, K., Ren, M., Liang, X., Peng, P., Sheng, G., Fu, J., 2008. Ecological risk assessment of thallium pollution in the surface sediment of Beijiang river. Ecol. Environ. 17, 528–532.

Guo, Y., Feng, X., Li, Z., He, T., Yan, H., Meng, B., Zhang, J., Qiu, G., 2008. Distribution and wet deposition fluxes of total and methyl mercury in Wujiang River Basin, Guizhou, China. Atmos. Environ. 42, 7096–7103.

Hissler, C., Probst, J.-L., 2006. Chlor-alkali industrial contamination and riverine transport of mercury: distribution and partitioning of mercury between water, suspended matter, and bottom sediment of the Thur River, France. Appl. Geochem. 21, 1837–1854.

Huang, Q., Chen, J., Huang, W., Reinfelder, J.R., Fu, P., Yuan, S., Wang, Z., Yuan, W., Cai, H., Ren, H., 2019. Diel variation in mercury stable isotope ratios records photoreduction of PM 2.5-bound mercury. Atmos. Chem. Phys. 19, 315–325.

Huang, Q., Liu, Y., Chen, J., Feng, X., Huang, W., Yuan, S., Cai, H., Fu, X., 2015. An improved dual-stage protocol to pre-concentrate mercury from airborne particles for precise isotopic measurement. J. Anal. Atom. Spectr. 30, 957–966.

Jiskra, M., Wiederhold, J.G., Bourdon, B., Kretzschmar, R., 2012. Solution speciation controls mercury isotope fractionation of Hg (II) sorption to goethite. Environ. Sci. Technol. 46, 6654–6662.

Jiskra, M., Wiederhold, J.G., Skyllberg, U., Kronberg, R.-M., Hajdas, I., Kretzschmar, R., 2015. Mercury deposition and re-emission pathways in boreal forest soils investigated with Hg isotope signatures. Environ. Sci. Technol. 49, 7188–7196.

Jiskra, M., Wiederhold, J.G., Skyllberg, U., Kronberg, R.-M., Kretzschmar, R., 2017. Source tracing of natural organic matter bound mercury in boreal forest runoff with mercury stable isotopes. Environ. Sci. Proc. Imp. 19, 1235–1248.

Kocman, D., Kanduč, T., Ogrinc, N., Horvat, M., 2011. Distribution and partitioning of mercury in a river catchment impacted by former mercury mining activity. Biogeochemistry 104, 183–201.

Kocman, D., Wilson, S., Amos, H., Telmer, K., Steenhuisen, F., Sunderland, E., Mason, R., Outridge, P., Horvat, M., 2017. Toward an assessment of the global inventory of present-day mercury releases to freshwater environments. Int. J. Environ. Res. Public Health 14, 138.

Kritee, K., Barkay, T., Blum, J.D., 2009. Mass dependent stable isotope fractionation of mercury during mer mediated microbial degradation of monomethylmercury. Geochem. Cosmochim. Acta 73, 1285–1296.

Kritee, K., Blum, J.D., Johnson, M.W., Bergquist, B.A., Barkay, T., 2007. Mercury stable isotope fractionation during reduction of Hg (II) to Hg (0) by mercury resistant microorganisms. Environ. Sci. Technol. 41, 1889–1895.

Leitch, D.R., Carrie, J., Lean, D., Macdonald, R.W., Stern, G.A., Wang, F., 2007. The delivery of mercury to the Beaufort Sea of the Arctic ocean by the Mackenzie river. Sci. Total Environ. 373, 178–195.

Leopold, K., Foulkes, M., Worsfold, P., 2010. Methods for the determination and speciation of mercury in natural waters—a review. Anal. Chim. Acta 663, 127–138.

Liu, J., Feng, X., Yin, R., Zhu, W., Li, Z., 2011. Mercury distributions and mercury isotope signatures in sediments of Dongjiang, the Pearl River Delta, China. Chem. Geol. 287, 81–89.

Liu, J., Feng, X., Zhu, W., Zhang, X., Yin, R., 2012. Spatial distribution and speciation of mercury and methyl mercury in the surface water of East River (Dongjiang) tributary of Pearl River Delta, South China. Environ. Sci. Pollut. Res. 19, 105–112.

Liu, J., Li, S., Chen, J., Zhong, J., Yue, F., Lang, Y., Ding, H., 2017a. Temporal transport of major and trace elements in the upper reaches of the Xijiang River, SW China. Environ. Earth. Sci. 76, 299.

Liu, M., Du, P., Yu, C., He, Y., Zhang, H., Sun, X., Lin, H., Luo, Y., Xie, H., Guo, J., 2017b. Increases of total mercury and methylmercury releases from municipal sewage into environment in China and implications. Environ. Sci. Technol. 52, 124–134.

Liu, M., Zhang, W., Wang, X., Chen, L., Wang, H., Luo, Y., Zhang, H., Shen, H., Tong, Y., Ou, L., 2016. Mercury release to aquatic environments from anthropogenic sources in China from 2001 to 2012. Environ. Sci. Technol. 50, 8169–8177.

Lyons, W.B., Fitzgibbon, T.O., Welch, K.A., Carey, A.E., 2006. Mercury geochemistry of the scioto river, Ohio: impact of agriculture and urbanization. Appl. Geochem. 21, 1880–1888.

Malinovsky, D., Vanhaecke, F., 2011. Mercury isotope fractionation during abiotic transmethylation reactions. Int. J. Mass Spectrom. 307, 214–224.

Mead, C., Lyons, J.R., Johnson, T.M., Anbar, A.D., 2013. Unique Hg stable isotope signatures of compact fluorescent lamp-sourced Hg. Environ. Sci. Technol. 47, 2542–2547.

Obrist, D., Kirk, J.L., Zhang, L., Sunderland, E.M., Jiskra, M., Selin, N.E., 2018. A review of global environmental mercury processes in response to human and natural perturbations: changes of emissions, climate, and land use. Ambio 47, 116–140.

Rodríguez-González, P., Epov, V.N., Bridou, R., Tessier, E., Guyoneaud, R., Monperrus, M., Amouroux, D., 2009. Species-specific stable isotope fractionation of mercury during Hg (II) methylation by an anaerobic bacteria (Desulfobulbus propionicus) under dark conditions. Environ. Sci. Technol. 43, 9183–9188.

Schuster, P.F., Striegl, R.G., Aiken, G.R., Krabbenhoft, D.P., Dewild, J.F., Butler, K., Kamark, B., Dornblaser, M., 2011. Mercury export from the Yukon River Basin and potential response to a changing climate. Environ. Sci. Technol. 45, 9262–9267.

Selin, N.E., 2009. Global biogeochemical cycling of mercury: a review. Annu. Rev. Environ. Resour. 34, 43–63.

Shao, D., Kang, Y., Cheng, Z., Wang, H., Huang, M., Wu, S., Chen, K., Wong, M.H., 2013. Hair mercury levels and food consumption in residents from the Pearl River Delta: South China. Food Chem. 136, 682–688.

Shao, D., Liang, P., Kang, Y., Wang, H., Cheng, Z., Wu, S., Shi, J., Lo, S.C.L., Wang, W., Wong, M.H., 2011. Mercury species of sediment and fish in freshwater fish ponds around the Pearl River Delta, PR China: human health risk assessment. Chemosphere 83, 443–448.

Sherman, L.S., Blum, J.D., Johnson, K.P., Keeler, G.J., Barres, J.A., Douglas, T.A., 2010. Mass-independent fractionation of mercury isotopes in Arctic snow driven by sunlight. Nat. Geosci. 3, 173.

Shi, J., Ip, C.C., Zhang, G., Jiang, G., Li, X., 2010. Mercury profiles in sediments of the

Pearl River Estuary and the surrounding coastal area of South China. Environ. Pollut. 158, 1974–1979.
Stoken, O.M., Riscassi, A.L., Scanlon, T.M., 2016. Association of dissolved mercury with dissolved organic carbon in US rivers and streams: the role of watershed soil organic carbon. Water Resour. Res. 52, 3040–3051.
Štrok, M., Baya, P.A., Hintelmann, H., 2015. The mercury isotope composition of Arctic coastal seawater. C.R. Geosci. 347, 368–376.
Sun, G., Sommar, J., Feng, X., Lin, C., Ge, M., Wang, W., Yin, R., Fu, X., Shang, L., 2016. Mass-dependent and-independent fractionation of mercury isotope during gas-phase oxidation of elemental mercury vapor by atomic Cl and Br. Environ. Sci. Technol. 50, 9232–9241.
Tavares, D.S., Lopes, C.B., Daniel-da-Silva, A.L., Vale, C., Trindade, T., Pereira, M.E., 2016. Mercury in river, estuarine and seawaters–Is it possible to decrease realist environmental concentrations in order to achieve environmental quality standards? Water Res. 106, 439–449.
Wang, Q., Kim, D., Dionysiou, D.D., Sorial, G.A., Timberlake, D., 2004. Sources and remediation for mercury contamination in aquatic systems—a literature review. Environ. Pollut. 131, 323–336.
Wang, S., Xing, D., Wei, Z., Jia, Y., 2013. Spatial and seasonal variations in soil and river water mercury in a boreal forest, Changbai Mountain, Northeastern China. Geoderma 206, 123–132.
Wang, Z., Chen, J., Feng, X., Hintelmann, H., Yuan, S., Cai, H., Huang, Q., Wang, S., Wang, F., 2015. Mass-dependent and mass-independent fractionation of mercury isotopes in precipitation from Guiyang, SW China. C.R. Geosci. 347, 358–367.
Washburn, S.J., Blum, J.D., Demers, J.D., Kurz, A.Y., Landis, R.C., 2017. Isotopic characterization of mercury downstream of historic industrial contamination in the South River, Virginia. Environ. Sci. Technol. 51, 10965–10973.
Washburn, S.J., Blum, J.D., Kurz, A.Y., Pizzuto, J.E., 2018. Spatial and temporal variation in the isotopic composition of mercury in the South River, VA. Chem. Geol. 494, 96–108.
Wiederhold, J.G., Cramer, C.J., Daniel, K., Infante, I., Bourdon, B., Kretzschmar, R., 2010. Equilibrium mercury isotope fractionation between dissolved Hg (II) species and thiol-bound Hg. Environ. Sci. Technol. 44, 4191–4197.
Woerndle, G.E., Tsz-Ki Tsui, M., Sebestyen, S.D., Blum, J.D., Nie, X., Kolka, R.K., 2018. New insights on ecosystem mercury cycling revealed by stable isotopes of mercury in water flowing from a headwater peatland catchment. Environ. Sci. Technol. 52, 1854–1861.
Xu, H., Sun, R., Cao, J., Huang, R., Guinot, B., Shen, Z., Jiskra, M., Li, C., Du, B., He, C., 2019. Mercury stable isotope compositions of Chinese urban fine particulates in winter haze days: implications for Hg sources and transformations. Chem. Geol. 504, 267–275.
Yuan, S., Chen, J., Cai, H., Yuan, W., Wang, Z., Huang, Q., Liu, Y., Wu, X., 2018. Sequential samples reveal significant variation of mercury isotope ratios during single rainfall events. Sci. Total Environ. 624, 133–144.
Yuan, S., Zhang, Y., Chen, J., Kang, S., Zhang, J., Feng, X., Cai, H., Wang, Z., Wang, Z., Huang, Q., 2015. Large variation of mercury isotope composition during a single precipitation event at Lhasa City, Tibetan Plateau, China. Proc. Earth Planet. Sci. 13, 282–286.
Zdanowicz, C.M., Krümmel, E., Poulain, A., Yumvihoze, E., Chen, J., Štrok, M., Scheer, M., Hintelmann, H., 2016. Historical variations of mercury stable isotope ratios in Arctic glacier firn and ice cores. Glob. Biogeochem. Cycles 30, 1324–1347.
Zhang, H., Yin, R., Feng, X., Sommar, J., Anderson, C.W., Sapkota, A., Fu, X., Larssen, T., 2013. Atmospheric mercury inputs in montane soils increase with elevation: evidence from mercury isotope signatures. Sci. Rep. UK. 3, 3322.
Zhao, L., Guo, Y., Meng, B., Yao, H., Feng, X., 2017. Effects of damming on the distribution and methylation of mercury in Wujiang River, Southwest China. Chemosphere 185, 780–788.
Zhen, G., Li, Y., Tong, Y., Yang, L., Zhu, Y., Zhang, W., 2016. Temporal variation and regional transfer of heavy metals in the Pearl (Zhujiang) River, China. Environ. Sci. Pollut. Res. 23, 8410–8420.
Zheng, W., Demers, J.D., Lu, X., Bergquist, B.A., Anbar, A.D., Blum, J.D., Gu, B., 2018. Mercury stable isotope fractionation during abiotic dark oxidation in the presence of thiols and natural organic matter. Environ. Sci. Technol. 53, 1853–1862.
Zheng, W., Foucher, D., Hintelmann, H., 2007. Mercury isotope fractionation during volatilization of Hg (0) from solution into the gas phase. J. Anal. Atom. Spectr. 22, 1097–1104.
Zheng, W., Hintelmann, H., 2009. Mercury isotope fractionation during photoreduction in natural water is controlled by its Hg/DOC ratio. Geochem. Cosmochim. Acta 73, 6704–6715.
Zheng, W., Hintelmann, H., 2010a. Isotope fractionation of mercury during its photochemical reduction by low-molecular-weight organic compounds. J. Phys. Chem. A 114, 4246–4253.
Zheng, W., Hintelmann, H., 2010b. Nuclear field shift effect in isotope fractionation of mercury during abiotic reduction in the absence of light. J. Phys. Chem. A 114, 4238–4245.
Zheng, W., Kang, S., Feng, X., Zhang, Q., Li, C., 2010. Mercury speciation and spatial distribution in surface waters of the Yarlung Zangbo River, Tibet. Chin. Sci. Bull. 55, 2697–2703.
Zheng, W., Obrist, D., Weis, D., Bergquist, B.A., 2016. Mercury isotope compositions across North American forests. Glob. Biogeochem. Cycles 30, 1475–1492.